Effect of ECAE on Microstructures and Mechanical Properties of Solution Heat Treated Mg–5(mass%) Sn Alloy

Hao-Jan Tsai[1], Chin-Guo Kuo[2], Chuen-Guang Chao[1,*] and Tzeng-Feng Liu[1]

[1]*Department of Materials Science and Engineering, National Chiao Tung University, Hsinchu 300, Taiwan*
[2]*Department of Industrial Education, National Taiwan Normal University, Taipei 162, Taiwan*

The microstructures and mechanical properties of the Mg–5(mass%) Sn alloy subjected to a solution heat treatment (SHT) were investigated by using equal channel angular extrusion (ECAE). The average grain size was significantly refined from 147 µm (as-cast) to 16 µm by ECAE four passes. Further, the fine Mg_2Sn particles were uniformly distributed in the matrix by dynamic precipitation after ECAE four passes. The yield strength (YS), ultimate tensile strength (UTS) and elongations also showed notable improvements at room temperature and high temperatures (100 and 200°C) on account of the ECAE process. Further, the tensile strength and elongations were better than those of the ECAE without SHT alloy. Those results show that SHT is a useful way to enhance the effect of ECAE on the mechanical properties of Mg–5(mass%) Sn alloy.   [doi:10.2320/matertrans.M2013088]

1. Introduction

Magnesium alloys are the lightest metals, which have the best specific rigidity among structural metals. They also have excellent heat dissipation and vibration resistance, which could easily be seen from that used in 3C products and automobile parts.[1] The most commercially employed magnesium alloys are the Mg–Al binary systems. The β-phase ($Mg_{17}Al_{12}$) is the main phase to increase the strength of AZ series magnesium alloys (AZ31, AZ61 and AZ91) at room temperature; however, the AZ series alloys also demonstrat a lower strength at high temperatures. Because the β-phase is clearly dissolved in the matrix at high temperature (120°C), increasing the high temperature properties is the most important issue.

Early reports studied the rare earth (RE) addition to magnesium alloys in order to improve the high temperature properties.[2–4] However, RE was an expensive element. In contrast, tin was an inexpensive element and easily obtained.

Recently, scholars studied the Mg–Sn based alloy system.[5–14] The Mg–Sn phase diagram showed that the melting point of the Mg_2Sn phase (770°C) within the matrix of Mg–Sn alloys was much higher than that of the $Mg_{17}Al_{12}$ phase (462°C) in Mg–Al alloys.[14] This fact could significantly improve the high temperature properties.

Sasaki *et al.* and Wei *et al.* studied the Mg–Sn–Zn and Mg–5(mass%) Sn alloys, respectively, to improve the creep behavior by using aging hardening.[8,9] In particular, the compressive creep resistance of aging treated Mg–5(mass%) Sn alloy was much better than that of the as-cast alloy with temperatures from 150 to 200°C at the applied stresses of 25 to 35 MPa.

Beside the aging treatment, some scholars focused on thermo-mechanical treatments to improve the mechanical properties of the Mg–Sn based alloys at high temperatures by obtaining grain refinement as the main strengthening treatment.[10–13] Sasaki *et al.* used the extrusion process to produce a fine grain structure at 250°C; thus, an ultimate tensile strength (UTS) of 354 MPa for the Mg–Sn–Zn–Al alloy was attained at room temperature.[11] Park *et al.* studied the Mg–8Sn–1Al–1Zn alloy.[12] The authors used the solution heat treatment (SHT) and indirect extrusion in a two-step process to produce ultra-fine grains (<10 µm). However, they focused on the superplastic properties of the alloy and did not investigate the high temperature strength of the alloy in detail. From the above references, it follows that the aging treatment and thermo-mechanical treatments were powerful ways to increase the high temperature mechanical properties of Mg–Sn alloys.

In our previous study, we investigated the microstructures and mechanical properties of the Mg–2,5,8 (mass%) Sn alloys at high temperatures after an ECAE process without SHT.[13] The results showed that the Mg–5(mass%) Sn alloy had the best mechanical properties at room temperature and high temperatures (100 and 200°C), as well as the mechanical properties clearly improved after ECAE four passes. The tin solubility in the α-Mg was demonstrated from the Mg–Sn binary phase diagram; the amount of tin solubility sharply dropped when the eutectic transformation temperature decreased from 561°C (14.85 mass%) to 200°C (0.45 mass%).[14] It provided a basis for improving the mechanical properties of Mg–5(mass%) Sn alloy via the SHT or aging treatment.

In the present study, we aim to produce grain refinement and make the distribution of Mg_2Sn particles more uniformly by using the SHT + ECAE two-step process. Furthermore, we attempt to increase the high temperature tensile strength and elongations of the Mg–5(mass%) Sn alloy.

2. Experiment Procedure

An Mg–Sn alloy with added tin levels of 5 mass% was prepared. Pure magnesium (99.95 mass%) and pure tin (99.98 mass%) were melted in a crucible under the protection of SF_6 flux at 800°C. The melted mixture was stirred to ensure homogeneity. This was held at 720°C for about 30 min

*Corresponding author, E-mail: cgchao@mail.nctu.edu.tw

and finally casted into a steel mould that was preheated to 250°C. The cavity dimensions of the mould were $300 \times 70 \times 60 \, mm^3$. The as-cast ingots were given solution heat treatment at 480°C for 22 h. The ECAE was conducted with a die having a 120 degree angled channel using the Bc processing route, in which the specimen was removed from the die and then rotated 90 degree in the same direction between each pass. The dimension of specimens was $15 \times 15 \times 70 \, mm^3$. The specimens were then extruded through four passes at a fixed temperature of 200°C with an extrusion rate about 2 mm/min. The ECAE temperature was controlled and maintained by thermocouple and digital temperature controller. If the temperature changing was detected by thermocouple, the digital temperature controller could feedback and adjust the ECAE temperature immediately.

The metallographic specimens were sliced at the same place in each as-cast, as-SHT and ECAE samples. Those specimens were polished and etched with a solution of 5 vol% nitric acid + ethyl alcohol. The microstructures of the Mg–5(mass%) Sn alloy was observed by an optical microscope (OM) and a scanning electron microscope (SEM). The tensile specimens were cut into slices having gauge length of 6 mm via the wire-electrode cutting process. The tensile tests were conducted at room temperature and at high temperatures (100 and 200°C) on a tensile testing machine (Instron8500) with a constant strain rate of $1 \times 10^{-3} \, s^{-1}$. The tensile direction (TD) was parallel to the extrusion direction (ED).

3. Results and Discussion

3.1 Microstructures of as-cast and states with SHT

Continuous eutectic α-Mg + Mg_2Sn layered precipitates could be found at the grain boundary of the as-cast Mg–5(mass%) Sn alloy as shown in Fig. 1(a). However, Fig. 1(a) also showed the difference of brightness near grain boundary. Figure 2(b) could explain this phenomenon. The SEM image demonstrated that a large number of fine Mg_2Sn particles distributed near the grain boundary; suggesting those Mg_2Sn particles which distributed near grain boundary caused the brightness difference. After the SHT at 480°C for 22 h, the microstructure of the Mg–5(mass%) Sn alloy significantly changed as shown in Fig. 1(c). The grain boundary was clean in the optical micrograph (OM) of the Mg–5(mass%) Sn alloy. It means that the continuous eutectic α-Mg + Mg_2Sn precipitates were dissolved in the matrix after water quenching.

3.2 Microstructures after ECAE process state

Figures 2(a)–2(c) showed the OM images of the Mg–5(mass%) Sn alloy after SHT + ECAE one, two and four passes. The microstructures distribution were homogeneous; the average grain size decreased with increasing ECAE passes from 147 µm (as-cast) to 16 µm (SHT + ECAE four passes).

Figures 2(d)–2(f) showed the SEM images of the Mg–5(mass%) Sn alloy after SHT + ECAE one, two and four passes. Figure 2(d) showed that the fine and discontinuous Mg_2Sn particles were precipitated through the dynamic precipitation during ECAE one pass. Further, the fine Mg_2Sn
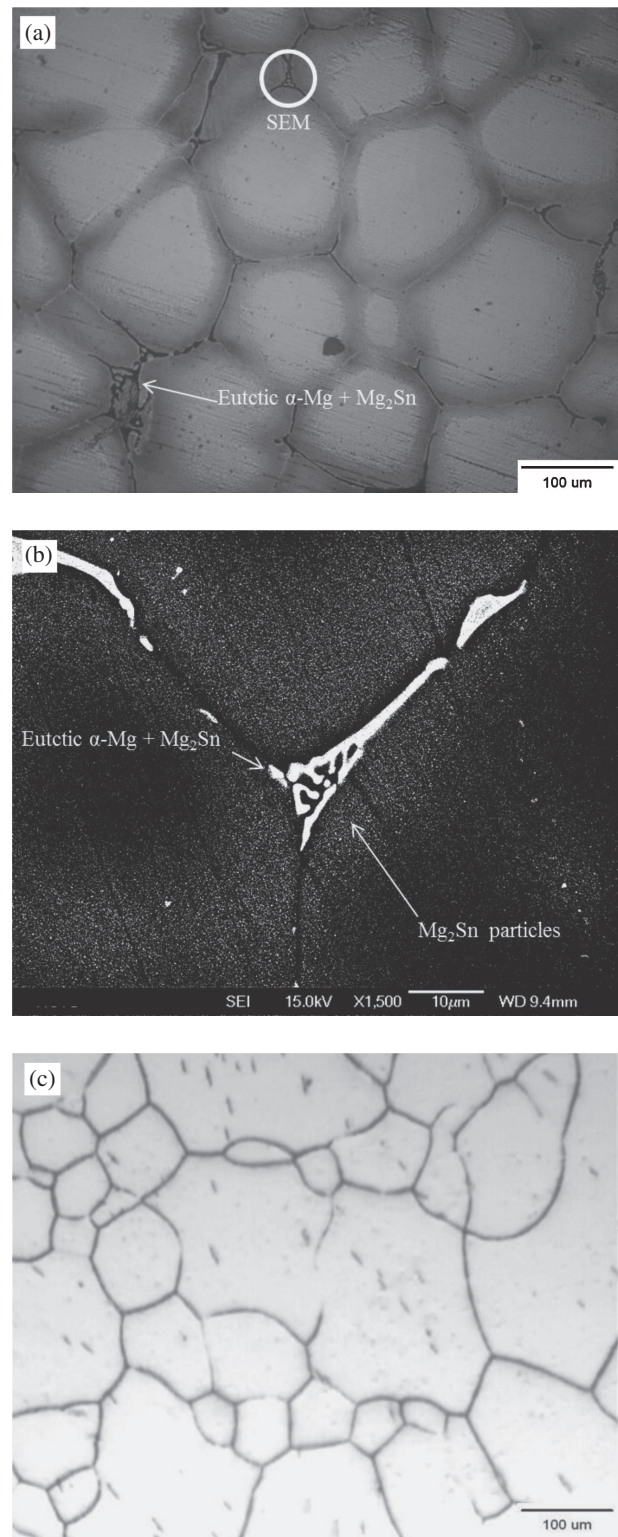

Fig. 1   OM and SEM images of Mg–5(mass%) Sn alloy (a) OM as-cast, (b) SEM as-cast and (c) OM as-SHT at 480°C for 22 h.

particles which distributed more uniformly were observed after ECAE two and four passes, as shown in Figs. 2(e) and 2(f).

Table 1 showed the average grain size of the Mg–5(mass%) Sn alloy with or none SHT after ECAE one, two and four passes. It was clear that the average grain size of the Mg–5(mass%) Sn alloy decreased with increasing ECAE
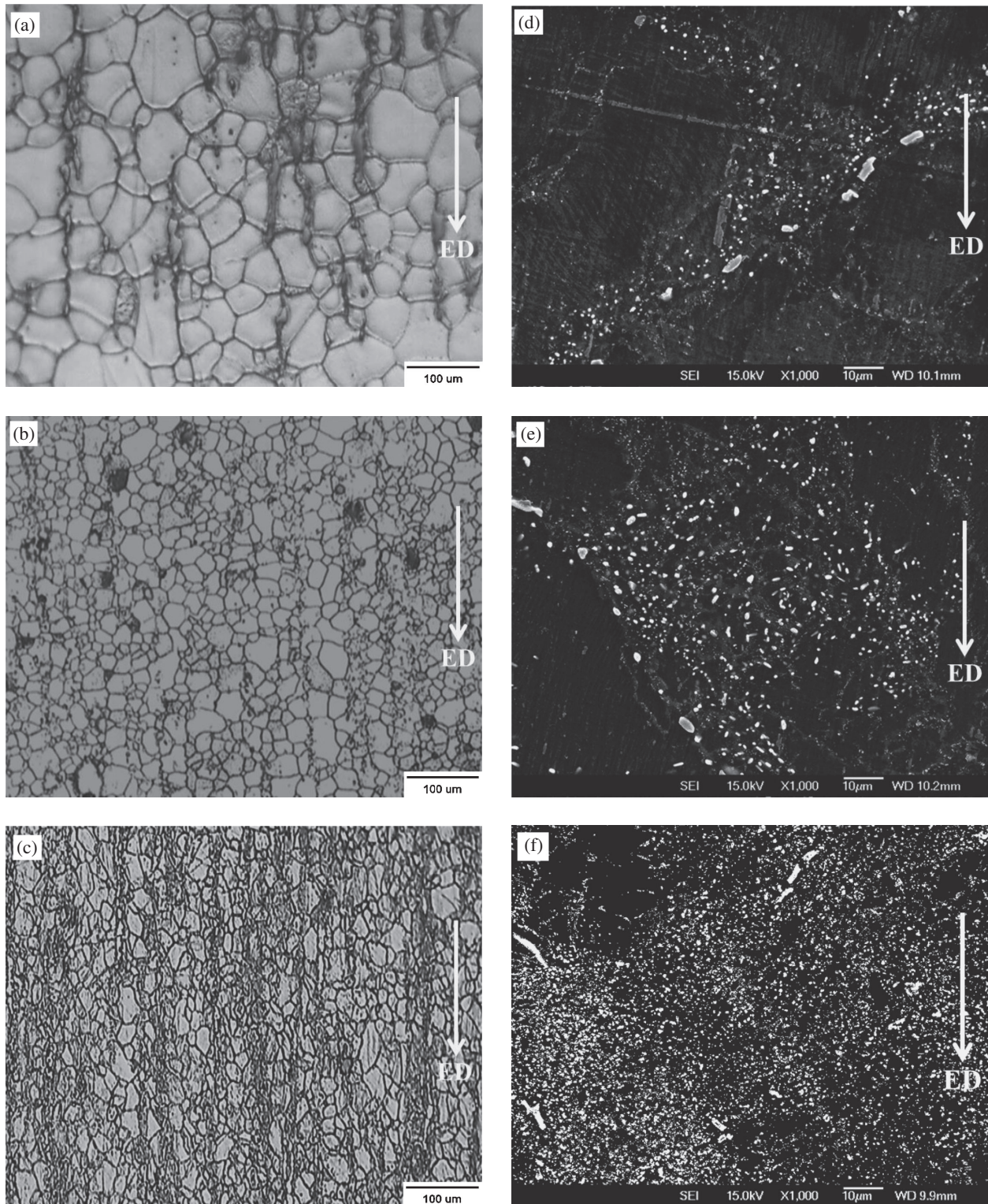
Fig. 2   Microstructures of Mg–5(mass%) Sn alloy after ECAE process (a) $N = 1$ after SHT, (b) $N = 2$ after SHT, (c) $N = 4$ after SHT, (d) $N = 1$ after SHT, (e) $N = 2$ after SHT and (f) $N = 4$ after SHT.

Table 1   Average grain size of Mg–5(mass%) Sn alloy.

As-cast		SHT + ECAE	ECAE none SHT
	$N = 1$	48.4 µm	87.5 µm
147.0 µm	$N = 2$	20.3 µm	69.7 µm
	$N = 4$	16.0 µm	28.0 µm

passes; further, the average grain size of Mg–5(mass%) Sn alloy with SHT was smaller than that of Mg–5(mass%) Sn alloy none SHT. There were two reasons for the decreasing in the average grain size.

First of all, the thermal energy and shear strain were helpful for the dynamic recrystallization (DRX); therefore, the DRX leaded to the production of fine grains. Secondly,

Table 2   Tensile properties of Mg–5(mass%) Sn alloy.

Samples	YS (MPa)	UTS (MPa)	Elongations (%)
as-cast*			
R.T	104	126	7.9
100°C	74	103	9.7
200°C	40	67	10.6
N = 4 none SHT*			
R.T	270	327	9.5
100°C	176	248	14.5
200°C	108	179	18.9
as-SHT			
R.T	142	175	4.3
100°C	106	134	6.2
200°C	76	99	7.1
N = 4 after SHT			
R.T	302	360	11.3
100°C	232	281	16.8
200°C	173	209	22.1

Strain rate = $1 \times 10^{-3}\,\text{s}^{-1}$. *: In our previous report.[13]

the as-SHT Mg–5(mass%) Sn alloy could dynamicly precipitate a large number of Mg_2Sn particles in the grain boundaries during the ECAE process at high temperature (200°C); further, those particles could retard grain boundary migration. Similarly, Park *et al.* reported that the thermally stable uniform precipitates at the grain boundaries inhibited grain growth during high temperature deformation.[17]

3.3 Tensile properties

Table 2 showed the tensile test results of the Mg–5(mass%) Sn alloy including as-cast, ECAE 4 passes none SHT, as-SHT and ECAE four passes after SHT. All the YS and UTS values increased after ECAE four passes at room temperature and high temperatures (100 and 200°C). The UTS of the Mg–5(mass%) Sn alloy after SHT + ECAE four passes significantly increased from 126 to 360 MPa at room temperature. Further, the UTS increased from 103 to 281 MPa at 100°C, as well as increased from 67 to 209 MPa at 200°C. In particular, the YS and UTS values after SHT + ECAE four passes were larger than those of Mg–5(mass%) Sn alloy ECAE four passes none SHT. For example, the UTS of the Mg–5(mass%) Sn alloy after SHT + ECAE four passes increased from 67 MPa (as-cast) to 209 MPa at 200°C, but the UTS increased from 67 MPa (as-cast) to 179 MPa at 200°C after ECAE four passes none SHT. Additionally, the YS and UTS of as-SHT were better than that of as-cast, but much poorer than that of SHT + ECAE four passes. Although the strength of as-SHT Mg–5(mass%) Sn alloy slightly increased by solid solution strengthening, the gains still maintained coarsening after SHT.

Moreover, the elongations of the Mg–5(mass%) Sn alloy including as-cast, ECAE 4 passes none SHT, as-SHT and ECAE four passes after SHT were also shown in Table 2. All the elongations of the Mg–5(mass%) Sn alloy after SHT + ECAE four passes, and after ECAE four passes none SHT displayed a similar trend. However, all the elongations of the Mg–5(mass%) Sn alloy after SHT + ECAE four

passes were larger than those of the alloy after ECAE four passes none SHT. The elongation of the Mg–5(mass%) Sn alloy increased slightly from 7.9 to 11.3% at room temperature after SHT + ECAE four passes. Further, the elongation increased from 9.7 to 16.8% at 100°C, and the elongation increased significantly from 10.6 to 22.1% at 200°C after SHT + ECAE four passes. On the other hand, all the elongations of the as-SHT Mg–5(mass%) Sn alloy were lower than that of ECAE four passes none SHT, and much lower than that of SHT + ECAE four passes.

From the above, a single SHT process could increase in limit the YS and UTS at room and high temperatures (100 and 200°C), but it was not enough to effectively promote the YS, UTS and elongations at the same time. By contrast, the SHT + ECAE two-step process were very helpful to enhance the strength and elongations of Mg–5(mass%) Sn alloy at room and high temperatures (100 and 200°C) because the ECAE process still played a key role to obviously increase the strength and elongations by grain refining and precipitates uniformly distribution.

3.4 Fracture surface

It was well known that a magnesium alloy failed in a brittle mode through cleavage or quasi-cleavage with an HCP structure at room temperature.[18] Figures 3(a)–3(c) were the fracture surfaces of Mg–5(mass%) Sn alloy samples after SHT + ECAE four passes. The tensile tests were conducted with a constant strain rate of $1 \times 10^{-3}\,\text{s}^{-1}$. Figure 3(a) showed that the fractures were due to the cleavage at room temperature and that several cleavages were present. Figure 3(b) showed the result at 100°C, which was similar to that at room temperature; the cleavage was the major fracture mode. Figure 3(c) showed that the specimen broke at 200°C. The result showed that the fracture surface consisted of dimples and cleavages. This means that the fracture mode of the Mg–5(mass%) Sn alloy gradually transformed from the brittle to the ductile through thermal activation. We further compared the fracture surface of as-cast, as-SHT and ECAE four passes none SHT conditions. Figures 3(d) and 3(e) showed that the fracture surface of as-cast and as-SHT broken at high temperature 200°C. The major fracture mode was cleavage and the large cracks were observed in the Figs. 3(d) and 3(e). Furthermore, we compared the fracture surface of Mg–5(mass%) Sn alloy after ECAE four passes none SHT in our previous report as shown in Fig. 3(f);[13] the fracture surface combined by a lot of cleavages and a few dimples. This result demonstrated that the Mg–5(mass%) Sn alloy after ECAE four passes none SHT had starting transformed from the brittle to the ductile at high temperature 200°C; however, the distribution area of dimples was less than that of SHT + ECAE four passes. This phenomenon indicated that the SHT + ECAE two-step process could significantly enhance ductile of the Mg–5(mass%) Sn alloy.

4. Conclusions

(1) The continuous eutectic α-Mg + Mg_2Sn precipitates were observed in the as-cast Mg–5(mass%) Sn alloy. The grain boundary was clean after SHT.
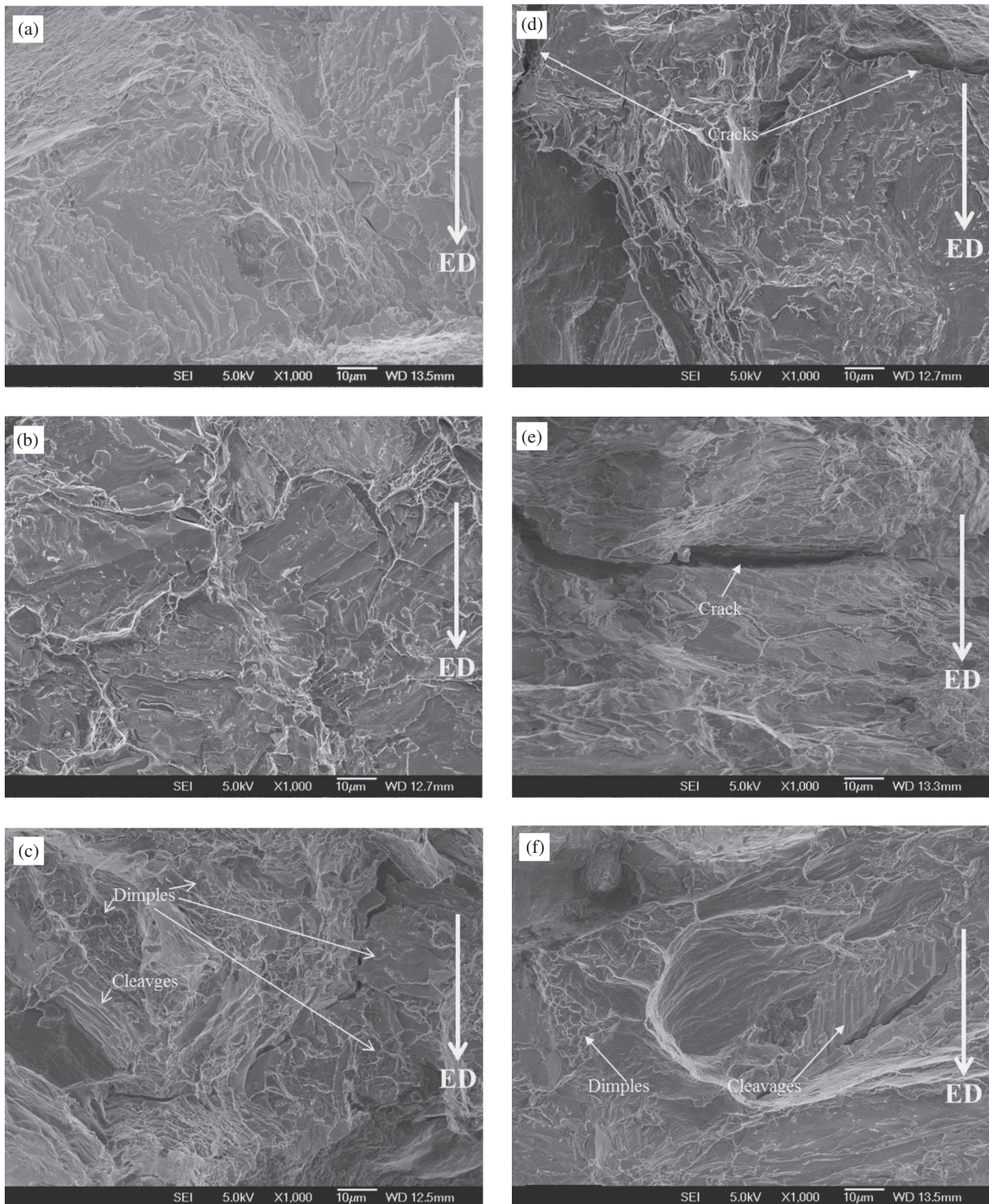
Fig. 3 Fracture surface after tensile test with a constant strain rate $1 \times 10^{-3}\,\mathrm{s}^{-1}$ (a) $N = 4$ after SHT broken at *RT*, (b) $N = 4$ after SHT broken at 100°C, (c) $N = 4$ after SHT broken at 200°C, (d) as-cast broken at 200°C, (e) as-SHT broken at 200°C and (f) ECAE four passes none SHT broken at 200°C.[13]

(2) The ECAE process was helpful for grain refining; the average grain size decreased with increasing ECAE passes from 147 µm (as-cast) to 16 µm (SHT + ECAE four passes).

(3) The fine and uniform Mg_2Sn particles of the as-SHT Mg–5(mass%) Sn alloy were produced by dynamic precipitation during ECAE process.

(4) The YS and UTS of the Mg–5(mass%) Sn alloy increased after SHT + ECAE four passes at room temperature and high temperatures (100 and 200°C).

(5) The fracture surface of the Mg–5(mass%) Sn alloy after SHT + ECAE four passes was due to cleavage at room temperature and 100°C, and the fracture surface consisted of dimples and cleavages at 200°C.

Acknowledgements

REFERENCES

1) Y. Kojima: Mater. Trans. **42** (2001) 1154–1159.
2) J. Gröbner and R. Schmid-Fetzer: J. Alloy. Compd. **320** (2001) 296–301.
3) Y. Wang, S. Guan, X. Zeng and W. Ding: Mater. Sci. Eng. A **416** (2006) 109–118.
4) W. Blum, P. Zhang, B. Watzinger, B. v. Grossmann and H. G. Haldenwanger: Mater. Sci. Eng. A **319–321** (2001) 735–740.
5) M. Bamberger: J. Mater. Sci. **41** (2006) 2821–2829.
6) D. H. Kang, S. S. Park, Y. S. Oh and N. J. Kim: Mater. Sci. Eng. A **449–451** (2007) 318–321.
7) C. L. Mendis, C. J. Bettles, M. A. Gibson and C. R. Hutchinson: Mater. Sci. Eng. A **435–436** (2006) 163–171.
8) T. T. Sasaki: Scr. Mater. **61** (2009) 80–83.
9) S. Wei, Y. Chen, Y. Tang, H. Liub, S. Xiao, G. Niu, X. Zhang and Y. Zhao: Mater. Sci. Eng. A **492** (2008) 20–23.
10) Y. V. R. K. Prasad, K. P. Rao, N. Hort and K. U. Kainer: Mater. Lett. **62** (2008) 4207–4209.
11) T. T. Sasaki, K. Yamamoto, T. Honma, S. Kamado and K. Hono: Scr. Mater. **59** (2008) 1111–1114.
12) S. S. Park and B. S. You: Scr. Mater. **65** (2011) 202–205.
13) H.-J. Tsai, C.-G. Kuo, C.-G. Chao and T.-F. Liu: Adv. Sci. Lett. **8** (2012) 599–604.
14) A. A. Nayeb-Hashemi and J. B. Clark: Bull. Alloy Phase Diagrams **5** (1984) 466–476.
15) A. Galiyev, R. Kaibyshev and G. Gottstein: Acta Mater. **49** (2001) 1199.
16) B. Somjeet, S. D. Satyaveer and S. Satyam: *Microstructure and Texture in Steels and Other Materials*, (Springer-Verlag, London, 2009) pp. 465–473.
17) S. S. Park, G. T. Bae, D. H. Kang, B. S. You and N. J. Kim: Scr. Mater. **61** (2009) 223–226.
18) Y. Lü, Q. Wang, X. Zeng, W. Ding, C. Zhai and Y. Zhu: Mater. Sci. Eng. A **278** (2000) 66–76.